ORIGINAL RESEARCH

Synthesis of Graphene Oxide Using Atmospheric Plasma for Prospective Biological Applications

Khurshed Alam[1,*]
Youn Yi Jo[2,*]
Chul-Kyu Park [iD][3]
Hoonsung Cho [iD][1]

[1]School of Materials Science & Engineering, Chonnam National University, Gwangju 61186, Republic of Korea; [2]Department of Anesthesiology and Pain Medicine, Gachon University, Gil Medical Center, Incheon 21565, Republic of Korea; [3]Gachon Pain Center and Department of Physiology, College of Medicine, Gachon University, Incheon 21999, Republic of Korea

*These authors contributed equally to this work

Correspondence: Chul-Kyu Park
Gachon Pain Center and Department of Physiology, College of Medicine, Gachon University, Incheon 21999, Republic of Korea
Tel +82-32-899-6692
Fax +82-32-724-9071
Email pck0708@gachon.ac.kr

Hoonsung Cho
School of Materials Science & Engineering, Chonnam National University, Gwangju 61186, Republic of Korea
Tel +82-62-530-1717
Fax +82-62-530-1699
Email cho.hoonsung@jnu.ac.kr

Introduction: This paper presents a novel technique for the synthesis of graphene oxide (GO) with various surface features using high-density atmospheric plasma deposition. Furthermore, to investigate the use of hydrophobic, super-hydrophobic, and hydrophilic graphene in biological applications, we synthesized hydrophobic, super-hydrophobic, and hydrophilic graphene oxides by additional heat treatment and argon plasma treatment, respectively. In contrast to conventional fabrication procedures, reduced graphene oxide (rGO) formed under low pressure and high-temperature environment using a new synthesis method—developed and described in this study—offers a convenient deposition method on any kind surface with controlled wettability.

Methods: High density at atmospheric plasma is used for the synthesis of rGO and GO and its biocompatibility based on various wetting properties was evaluated using MTT (3-(4,5-dimethylthiazol-2-yl)-2,5-diphenyltetrazolium bromide) assay, and the viability of cells in response to rGO and GO with various surface features was investigated. Structural integrity was characterized by Raman spectroscopy, FESEM and FE-TEM. Wettability was measured via contact angle method and confirmed with XPS analysis.

Results: We found that GO coating with a hydrophilic feature is more biocompatible than other surfaces as observed in case of fibroblast cells. We have shown that wettability—controlled by GO deposition—influences biocompatibilities and antibacterial effect of biomaterial surfaces.

Discussion: Measuring the contact angle, it is found that contact angle for hydrophobic is increased to 150.590 and reduced to 11.580 by heat and argon plasma treatment, respectively, from 75.880 that was initially in the case of hydrophobic surface. XPS analysis confirmed various oxygen-containing functional groups transforming as deposited hydrophobic surface into superhydrophobic and hydrophilic surface. Thus, we have proposed a new, direct, cost-effective, and highly productive method for the synthesis of rGO and GO—with various surface properties—for biological applications. Similarly, for the dental implant application, the *Streptococcus mutans* was used as an antibacterial effect and found that *S. mutans* grows slowly on hydrophilic surface. Thus, antibacterial effect was prominent on GO with hydrophilic surface.

Keywords: reduced graphene oxide, graphene oxide, atmospheric plasma, biocompatibility, MTT assay, hydrophobicity, super-hydrophobicity and hydrophilicity

Introduction

Materials made of carbon are recognized to be more biocompatible than inorganic materials.[1] Graphene—one of the allotropic forms of carbon—has unique properties that can be used in transparent conductive electrodes, photodetectors and transistors, light-emitting diodes, photoelectrochemical, and biological usages.[2] The

numerous chemical properties of graphene have enabled its applications in high-performance devices that generate and store energy. Recently, the applications of graphene, graphene oxide (GO), and reduced graphene oxide (rGO) have increased in the biomedical areas such as cell differentiation and osteoblast growth.[3–8] As compared to graphene, the presence of oxygen-containing functional groups in GO has promoted a wider application of the latter in the field of surface chemistry. Structurally, GO consists of a single layer of graphene sheets where the concentration of carbon atoms is reduced to 40–60% due to the addition of oxygen-containing functional groups.[9] Despite having multiple advantages over graphene, GO is still structurally defective and mechanically poorer. Further, GO can be modified into rGO by thermal or chemical reductions; rGO is an intermediate structure between the highly oxidized GO and ideal graphene, and thus, possesses some of the properties of both GO and graphene.[9]

GO is usually synthesized by exfoliating the bulk graphite, either mechanically or chemically, followed by their deposition on a designated substrate using chemical vapor deposition (CVD) on the metal catalyst and Hummer's technique.[9–12] GO is generated mechanically by exfoliating the bulk graphite using "scotch tape." This method is easier, however, the yield is low and it is difficult to control the layer thickness and quality of graphene due to the possible contaminations from surfactants or solvents, apart from being costlier and time-consuming.[9–11] Additionally, the layers are not deposited with uniformity. Generally crumples and ripples appear during the deposition of exfoliated layers on a substrate of interest, creating deformation of stacked layers.[13] CVD for GO synthesis is complicated and costlier and is further hindered by the generation of uncontrollable yield and higher energy demands.[11,14,15] The most extensive method for GO synthesis is Hummer's process.[16–19] However, this technique has been criticized due to the release of toxic gases like NO_2, N_2O_4, and ClO_2, which are explosive in nature.[20–23] The synthesis method discussed here is a relatively efficient technique that demonstrates a new means for synthesizing rGO and GO from a gaseous source, such as a mixture of methane (10%) and argon (balanced), in a very simple way. This simple process could be used for a cost-optimized synthesis of both rGO and GO.

Herein, we developed a novel method for the syntheses of rGO and GO with various surface properties i.e., hydrophilic, hydrophobic, and super hydrophobic, using a high-density atmospheric plasma instrument at ambient environment without using any catalyst for the effective deposition on various substrates. Hydrophobic rGO was synthesized by direct deposition using a mixture of methane and argon gas while super hydrophobic and hydrophilic GO were synthesized after treatment with additional heat and argon plasma, respectively.

A high-profile research is carried out on graphene and its derivatives in biological applications.[24–26] In some in vivo and in vitro studies both graphene and GO did not show cytotoxicity to bones.[27] In another in vitro study done on glioma Cells, it is found that GO is less toxic than rGO. However, the in vivo results show that toxicity is varied with graphene surface.[28] Impurities play a prominent factor in the biocompatibility of GO in in vitro and in vivo, so as highly purified GO in comparison with prepared GO shows minor negative effects.[29] Similarly in vitro study using magnetic graphene oxide exhibits low cytotoxicity.[25] So, to develop a relationship of GO with various surface properties we made an initial effort on in vitro study with fibroblast cells (NCTC L929) and anti-bacterial effect (*Streptococcus mutans*).

Materials
Synthesis of Reduced Graphene Oxide

Titanium specimens, having 2 mm thickness and 15 mm diameter, were polished by a series of sand papers and with alumina suspension (1 μm alumina powder). Before depositing rGO, the surface was ultrasonically cleaned with ethanol and distilled water for 10 minutes to remove the contaminants. GO was deposited using high-density atmospheric plasma generator PGS-300 (Expantech Co., Suwon, Korea), operated at 900 MHz. The plasma was generated with 100 W (900 MHz) power. Argon gas was used as a plasma carrier at a rate of 6 L/m. Then a mixture of methane (10%) and argon gas as a carbon source were introduced to the plasma at a rate of 100 SCCM while simultaneously increasing the power to 180 W. The change of plasma color indicates that source gas dissociation has started for carbon-carbon nucleation. The effects of distance between the plasma tip and the substrate on the deposition of GO was also evaluated. The plasma with the carbon source was run for 4 minutes for direct deposition of rGO on titanium substrate with the hydrophobic feature as illustrated in Figure 1. Furthermore, super-hydrophobicity and hydrophilicity were achieved after
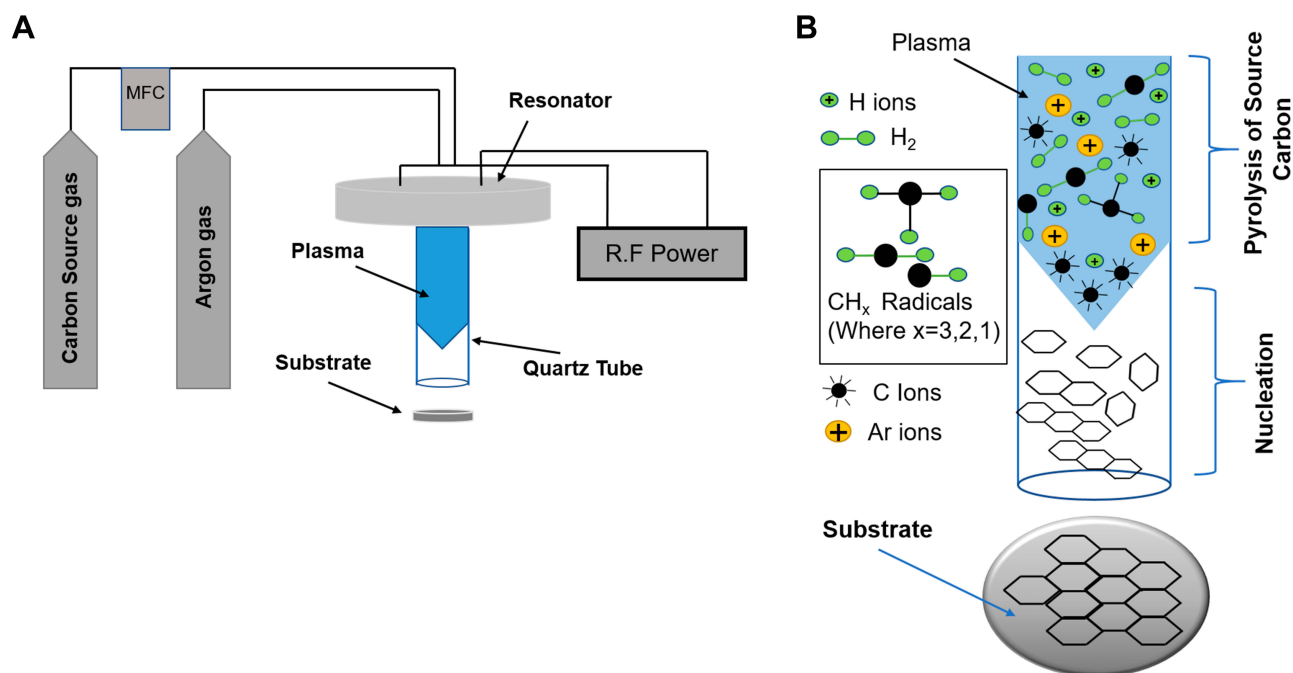
A

B

Figure 1 (**A**) Schematic diagram of the atmospheric plasma instrument. (**B**) Decomposition of methane in the high-dense plasma and carbon-carbon bonding through the tube.

additional heat treatment and argon plasma treatment, respectively.

Synthesis of Graphene Oxide

Here again substrate used is titanium with 2 mm thickness and 15 mm diameter and followed with the same procedure done for rGO synthesis but here we just treat the already deposited rGO with only argon plasma treatment at a rate of 6 L/m for 1 min and 30 sec with the source gas turned off.

Characterization of the Materials

The structural integrity of the direct deposition of rGO was confirmed through Raman spectroscopy, X-ray photoelectron spectroscopy (XPS), and field emission transmission electron microscopy (FE-TEM). We measured the transition from hydrophobic to hydrophilic and super hydrophobic by the contact angle (Phoenix 300, SEO Korea) that reflects the interaction of the surface with an aqueous solution. XPS was performed to differentiate between graphene oxide and reduced graphene oxide that reveal different oxygen-content of functional groups which changes as a hydrophobic surface transforms into super-hydrophobic or hydrophilic. Raman spectroscopy assured that both rGO and GO were successfully synthesized.

For biological applications, wettability plays an important role, and it was measured accordingly. Further, the biocompatibility of GO and rGO (having different surface properties ie, super hydrophobic, hydrophobic, or hydrophilic) deposited on titanium substrate was evaluated by MTT assay, to compare between carbon coating having different surface properties and bare titanium substrate. Cell viability is dramatically enhanced on the hydrophilic surface when compared with hydrophobic, super hydrophobic or titanium substrate.

In this paper, therefore, we proposed a highly productive and cost-effective novel technique for the direct deposition of rGO and GO, with various surface properties, on a biomedical substrate. We subsequently evaluated the biological application to confirm the relationship between different surface properties with cell viability and anti-bacterial effect.

Field Emission Transmission Electron Microscopy

Morphology of the GO-coated samples were analyzed by field emission transmission electron microscopy (FE-TEM, Model: JEM-2100F, JEOL LTD) using an acceleration voltage of 200 kV.

Field Emission Scanning Electron Microscopy

In order to study the surface roughness, we performed field emission scanning electron microscopy (FESEM, Model:

Gemini 500 + EDS (Oxford)) analyzing side view of the coatings.

Laser Raman Spectroscopy

Laser Raman spectroscopy (NRS-5100) was used at a wavelength of 532 nm in order to differentiate between rGO and GO.

High-Performance X-Ray Photoelectron Spectroscopy

High-Performance X-ray photoelectron spectroscopy (XPS, Model: K-ALPHA +) with Al Kα X-ray analyzer was used to study the various functional groups.

Contact Angle Instrument

Contact angle instrument is used to measure the wettability using distilled water (Phoenix 300, SEO Korea).

Thermo Scientific Varioskan Lux Spectrophotometer

Spectrophotometer is used for MTT assay evaluation at 570 nm.

Biocompatibility Assay

NCTC L929 cells (purchased from ATCC) were chosen for cells viability. In brief, L929 cells were seeded at a density of 5×10^4 cells/well (25% confluency) using 24 well plates in 1 mL RPMI media on GO and rGO coated surfaces with various surface properties and allowed the cells to settle down for attachment for a period of 3 days at 37°. After three days of incubation, media was removed with proper care and washed with 1x Phosphate Buffered Saline (PBS) twice. Next step is followed with 0.1mg/mL MTT (3-(4, 5-dimethylthiazol-2-yl)-2, 5-diphenyltetrazolium bromide) while putting 450ul RPMI media and 50ul MTT assay in each well. Further plates were incubated for at least 2 hours and then the media was replaced with 500ul MTT solvent (Dimethylsulfoxide). The absorbance was taken at 570 nm using Varioskan lux reader. Additionally, as a successful candidate for the surface treatment of the dental implant, *Streptococcus mutans* is used for antibacterial effect.

Results and Discussion

Raman spectroscopy analysis was performed to differentiate between rGO and GO and to find the number of layers as well. The characteristic peaks for graphene are D (1350 cm^{-1}), G (1580 cm^{-1}), and 2D peak at 2690 cm^{-1}. Pristine graphene does not have a D peak that represents defects, edges of a graphene crystal, and

chemical bonds.[30] Typical Raman spectra for GO are characterized by its D and G band corresponding to 1353 cm^{-1} and 1605 cm^{-1}, respectively,[31] The two major peaks for rGO arise at 1350 cm^{-1} and 1599 cm^{-1}, which corresponds to the D and G peak, respectively. However, rGO and GO can be differentiated by the variation observed in the ratio of D and G peak intensities (I(D)/I(G) ratio).[32] The I(D)/I(G) ratio was higher for rGO, suggesting high sp^2 clusters than GO.[32] The D peak arises due to the breathing mode of k-point photons of A$_{1g}$ symmetry, while the G band is due to the first-order scattering of E$_{2g}$ phonons that arise from sp^2 carbon atoms.[33,34]

Firstly, we evaluated the rate of synthesis and deposition of GO on the substrate based on the distance between the plasma and the substrate. The spectrum in Figure 2A does not show D, G, and 2D peaks, signifying that no carbon coating was done while the flame touches the substrate. Raman spectra of Figure 2B showed D, G, and 2D bands, transpired at 1348 cm^{-1}, 1592 cm^{-1}, and 2693 cm^{-1}, respectively confirming that rGO was successfully deposited at a distance of 2.5 cm. Similarly, D, G, and 2 D bands, for Figure 2C occurred at 1351 cm^{-1}, 1598 cm^{-1}, and 2692 cm^{-1}, respectively, which showed that rGO coating was successfully synthesized at a distance of 5 cm. Figure 2D has two prominent peaks at 1354 cm^{-1} and 1613 cm^{-1} corresponding to D, and G band, respectively that matches with the peaks of GO. The 2 D band was reduced with increasing flame distance, leading to the synthesis of GO. This phenomenon is attributed that adequate distance is required in the synthesis of GO because longer distance would enhance the presence of oxygen atoms during carbon-carbon bonding inside the tube as our process is atmospheric plasma based. The intensities were found to differentiate between rGO and GO using I$_{(D)}$/I$_{(G)}$ ratio and I(2D)/I(G) ratio that reflected the number of layers. The intensities, as shown in Figure 2B, are 457, 393, and 312 corresponding to D, G, and 2 D band, respectively, and the intensity ratio for I(2D)/I(G) was 0.79 showing a multi-layered rGO.[35] The intensities, shown in Figure 2C are 308, 291, and 281 for D, G, and 2 D peaks, respectively and its ratio for I(2D)/I(G) is 0.96 that corresponds to a multi-layered rGO.[35] Similarly, the intensities shown in Figure 2D are 455, 462, and 390 and the intensity ratio for I(2D)/I(G) was 0.84 corresponding to a multi-layered deposition of GO.[35] Likewise, the I$_{(D)}$/I$_{(G)}$ ratio for Figure 2B–D is 1.1; 1.0 and 0.9. On the basis of the I$_{(D)}$/I$_{(G)}$ ratio, Figure 2B and C are attributed to rGO while Figure 2D is assigned to GO.[32]
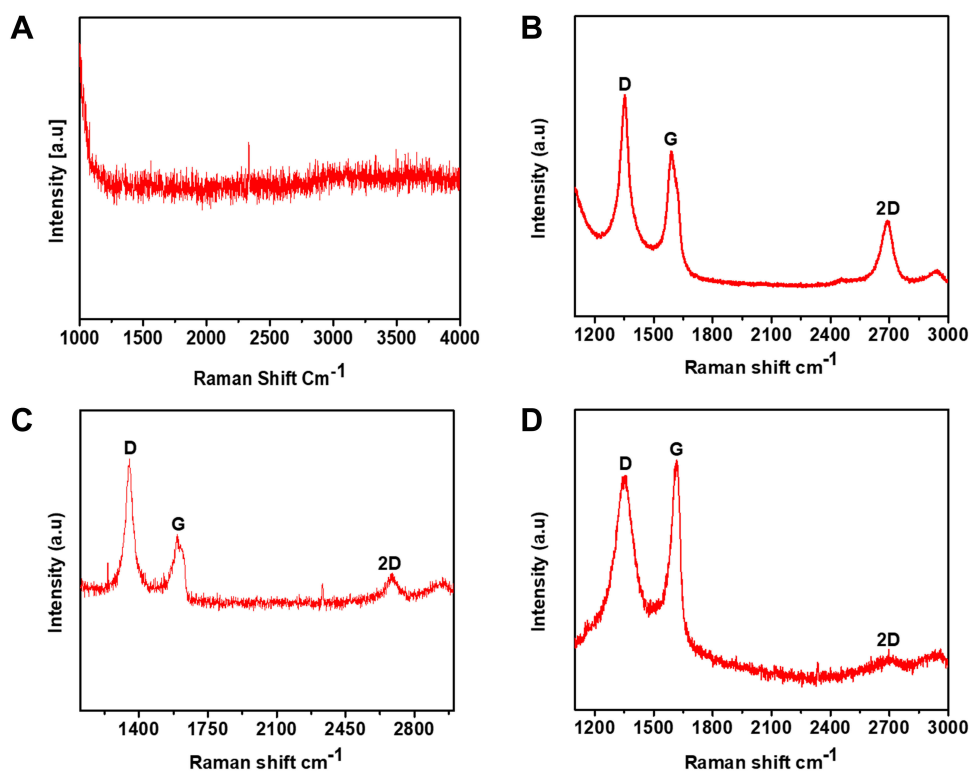
Figure 2 (**A**) No carbon coating while the flame is touched with the substrate. (**B**) rGO coating at a distance of 2.5 cm. (**C**) GO coating at a distance of 5 cm. (**D**) GO at a distance of 8 cm.**Abbreviations:** GO, graphene oxide; rGO, reduced graphene oxide.

X-ray photoelectron spectroscopic analyses were performed to identify the various functional groups in hydrophobic rGO, super-hydrophobic rGO, and hydrophilic GO. High-resolution XPS C1s spectra obtained for rGO and GO are shown in Figure 3. The C1s peak in Figure 3A belongs to rGO with hydrophobic features showing peak binding energies at 284.6, 285.3, and 286.4 eV ascribed to C=C (75.9 at. %), C-OH (12.57 at. %), and C-O-C (11.49 at. %), respectively.[36,37] Figure 3B is associated with rGO functionalized by additional heat treatment after direct deposition, thus generating super-hydrophobicity. The functional groups of the super-hydrophobic rGO, appeared at binding energies of 284.6, 285.4, and 286.48 eV attributed to C=C (77.875 at. %), C-OH (14.19 at. %), and C-O-C (7.93 at. %) respectively.[36–39] On the contrary, hydrophobic rGO was turned into GO with hydrophilic charters by additional argon plasma treatment. The transition from hydrophobic to hydrophilic was achieved due to the diverse precursors of plasma treatment. Various functional groups revealed in Figure 3C are 284.58, 285, 286.9, and 288.76, corresponding to C=C (40.4 at. %), C-OH (38.68 at. %), C-O-C (12.32 at. %), and COOH (8.96 at. %) respectively.[36–38] In Table 1 it is shown that O/C ratio

is the highest and the lowest at the hydrophilic and the super-hydrophobic surfaces respectively which confirms that hydrophilicity comes due to high amount of oxygen contents.

Furthermore, Figure 4 shows high-resolution spectra of O1s and N1s. Figure 4A shows two functional groups at about 533.3 eV and 532.38 eV assigned to C-O and C=O, respectively, which belongs to rGO with hydrophobic character, functional groups binding energies are well-matched with XPS database.[40] Figure 4B also shows two functional groups revealed at 532.5 eV and 531.6 eV, corresponding to C=O. The addition of carbonyl group indicates rGO with super-hydrophobicity.[36,40] Likewise, the peak in Figure 4C is also split into two components of COOH at 532.9 eV and C-O (epoxy) at 532.4 eV, which matched the peak of GO with hydrophilic feature.[37,41] Similarly, the peak shown in Figure 3D is the N1s peak that was additionally added in GO (hydrophilic) after argon plasma treatment as our synthesis process was operating in an open environment. The peak is split into two components, cyanide (N≡C) at 399.7 eV and NH$_2$ at 401.4 eV.[42,43]
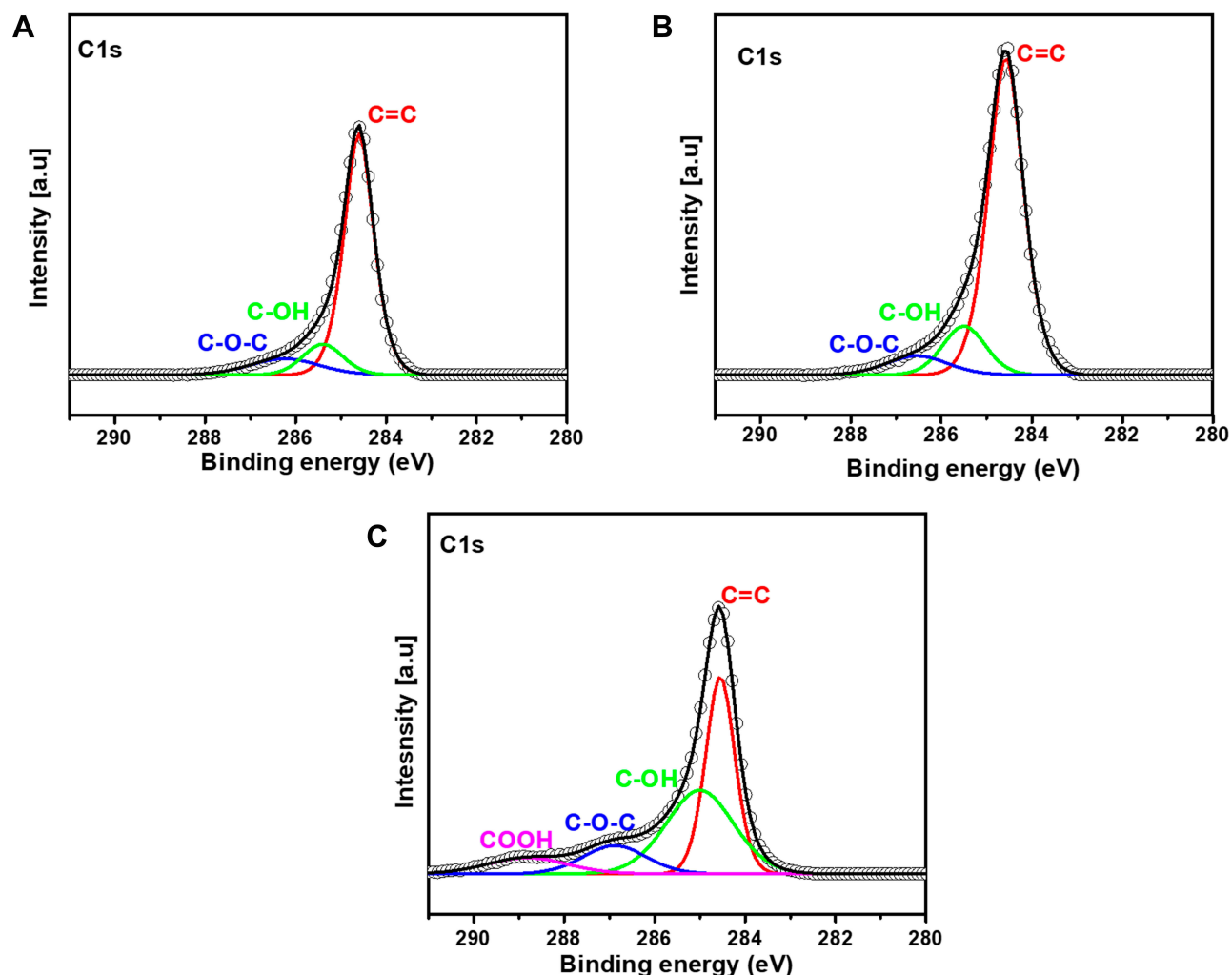
Figure 3 C1s peak of (**A**) rGO (Hydrophobic) obtained by direct deposition, (**B**) rGO (Super-Hydrophobic) obtained by additional heat treatment, (**C**) GO (Hydrophilic) obtained by additional argon plasma treatment after direct deposition.

Figure 5 shows TEM images obtained for rGO after direct deposition. In order to examine its morphology, the images were obtained through FE-TEM to confirm that reduced graphene oxide is synthesized. In Figure 5A, the layers are smoothly stacked one above the other with no ripples and crumples due to the smooth deposition by stable plasma. The appearance of these crumples usually appears during exfoliation and restacking processes that create the deformation of the stacked layers.[45] Figure 5B shows that rGO contains multi-layers in a similar direction and the inset is selected area diffraction showing polycrystalline structure.[21] Thus, morphology of rGO was confirmed through FE-TEM.

Figure 6 shows SEM side view images of both rGO and GO. These SEM images were taken to study the irregularities on the surface and it is evident from Figure 6 that rGO with hydrophobic surface is having some irregularities and GO with hydrophilic feature is smoothly deposited on the

Table I Atomic Percentages of C, O, O/C Ratio and Functional Groups

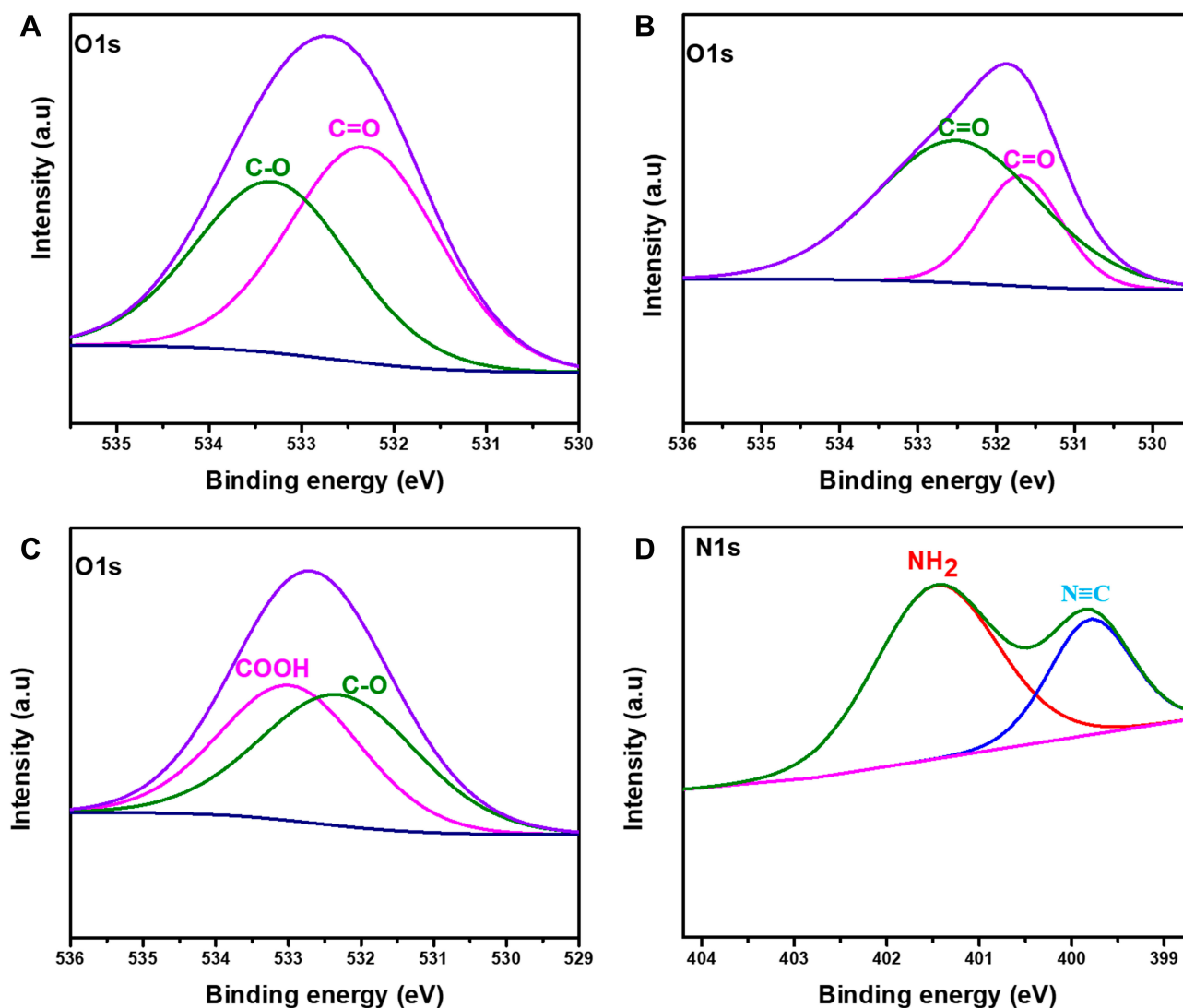| rGO and GO Coating	At % of C	At % of O	O/C Ratio	% of C=C	% of C-OH	% of C-O-C	% of COOH
Super Hydrophobic	90	10	0.11	77.8	14.19	7.93	
Hydrophobic	86.79	13.29	0.15[44]	75.9	12.57	11.49	
Hydrophilic	83	17	0.20	40.4	38.68	12.32	8.96

Figure 4 O1s and N1s peaks (**A**) O1s peak of rGO (Hydrophobic) obtained by direct deposition, (**B**) O1s peak of rGO (Super-Hydrophobic), (**C** and **D**) O1s and N1s peaks of GO (Hydrophilic).

surface. Thus, argon plasma treatment is helpful in transforming the surface from roughness into smoothness.

The wettability of carbon-coated samples (rGO and GO) is a crucial factor in the biological applications. Thus, wettability was measured through contact angle instrument (Phoenix 300, SEO Korea). Hydrophobicity is shown in Figure 7A, where reduced graphene oxide was directly deposited. Figure 7B shows super hydrophobicity where deposited carbon coating was heat-treated at 200 °C for 1 hour and 30 minutes. This remarkable increase in contact angle is attributed to the removal or reduction of oxygen-containing functional groups in graphene oxide sheets.[46] Figure 7C shows hydrophilic characters where the carbon-coated surface is additionally treated with argon plasma. The decrease in contact angle can be

ascribed to the addition of oxygen-containing functional groups that make hydrogen bonds with water molecules, as explained in Figure 3C through XPS analysis. Figure 7D shows the water droplet on bare titanium without carbon coating. All surface conditions are measured three times and the average and the standard deviation of the surfaces are described in Table 2.

Therefore, it is attributed that the transition from hydrophobicity to hydrophilicity is obtained after argon plasma treatment that helps in forming oxygen-containing functional groups, which makes the carbon deposited material more hydrophilic. The transition of rGO surfaces from hydrophobic to hydrophilic is simple and certain with a cost-optimized way without having additional requirements of temperature and vacuum
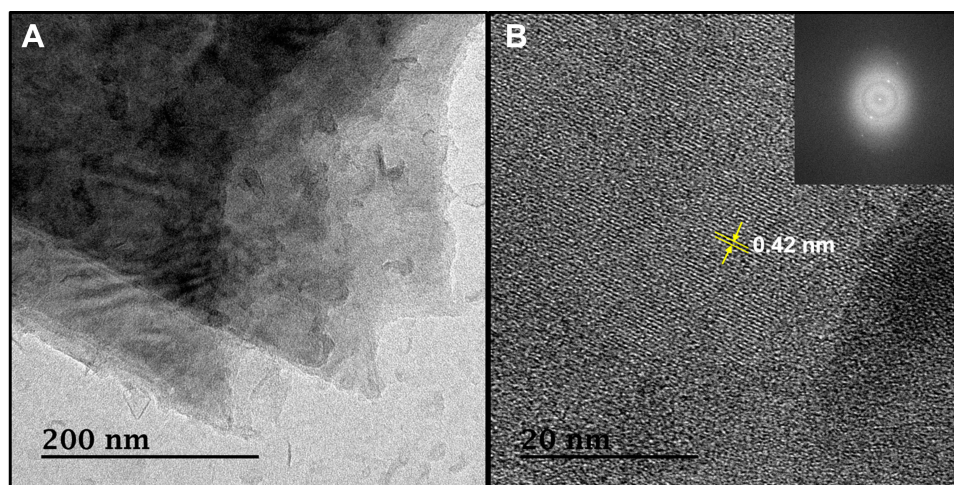
Figure 5 Field emission transmission electron microscopic images of reduced graphene oxide synthesized by atmospheric plasma. (**A**) Showing transparent sheets stacked one above the other. (**B**) Multi-layers and Selective area electron diffraction image (inset).
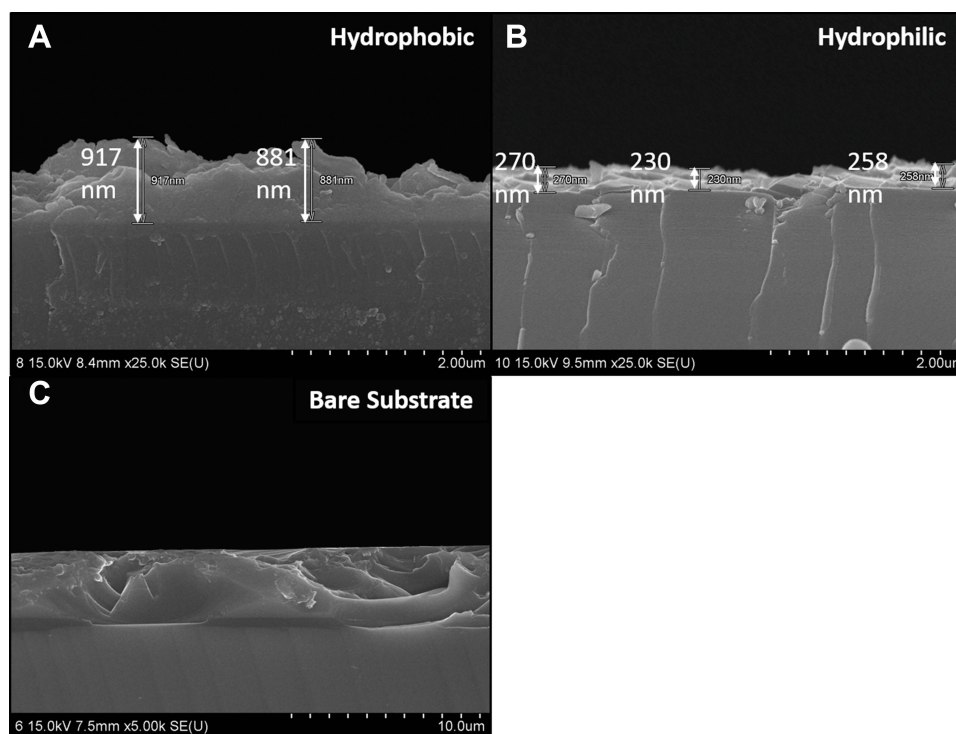

Figure 6 Field emission scanning electron microscopic images of rGO and GO. (**A**) rGO with hydrophobic surface. (**B**) GO with hydrophilic surface. (**C**) Substrate without coating.

formation. The mechanism involved behind the formation of hydrophilic surface is that the ion energy in plasma, usually greater than 10 eV, exceeds the binding energy of carbon, which is about 2.7 eV and 3.6 eV for π-bonding and σ-bonding respectively, thus forming an oxygen-containing functional groups.[11] Compounds like C-OH, C-O-C, COOH, C-O-C, and carboxylates (O-C=O) make the surface hydrophilic from hydrophobic due to

a dynamic interaction with water by generating intermolecular forces called hydrogen bonding.[47–50] The superhydrophobic features may resulted due to lack of these polar functional groups and presence of phenolic functional group that do exist at a higher temperature and possesses low solubility with water.[51]

Carbon deposition on the surface of titanium with various surface conditions (hydrophobic; Superhydrophobic;
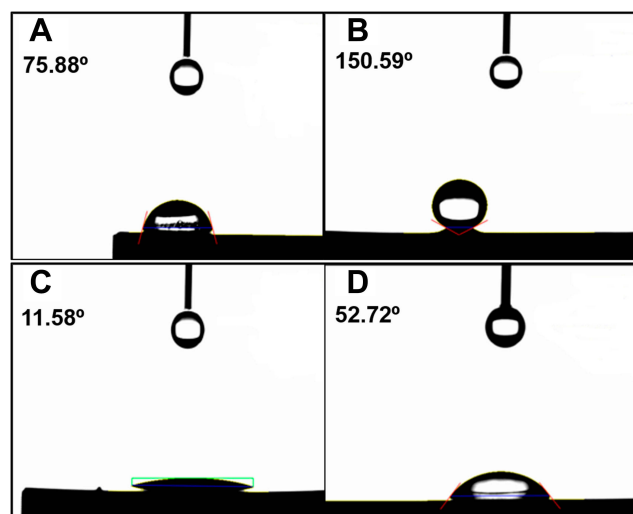
Figure 7 Water droplet on the surface of (**A**) Carbon layers deposited without plasma treatment. (**B**) Carbon layers deposited with additional heat treatment. (**C**) Carbon layers deposited with additional plasma treatment. (**D**) Without coating.

Figure 8 MTT assay for cytotoxicity of various surface conditions on Ti.

hydrophilic and bare Ti substrate) for the evaluation of biocompatibility was followed by seeding NCTC L929 fibroblast cells at 25% confluency (5 x 10^4/mL). After three days of growth, cell viability was evaluated by MTT assay (Figure 8). In this context, we found that carbon coating with hydrophilic feature proved to be a far better surface than other surface conditions. We observed entrapped air in the interfaces of the superhydrophobic coating due to a high contact angle of about 150.6, as shown in Figure 7B, implying that cells were not allowed to settle down appropriately on the surface. Similar observation was made with hydrophobic coating; however, it was less effective than the super-hydrophobicity. However, this effect was negligible in case of hydrophilic coating that resulted in higher cell viabilities. Similar phenomenon is observed by another group where they have defined that the air entrapped on superhydrophobic interfaces inhibit the cells growth and can negatively affect the adsorption process. Additionally, it is further defined that hydrophilic and

hydrophobic surfaces have a paramount role in the adhesion process of cells which is in consistent with our results.[52] So, neither rGO nor GO show any cytotoxicity, and the hydrophilic surface is more adequate for NCTC L929 fibroblast cell growth. As a successful candidate for the surface treatment for the dental implant, the antibacterial effect of the deposited graphene oxide was conducted (Figure 9). For this, *Streptococcus mutans* was incubated in the samples with various surface conditions (cell culture well-plates for the control, the bare surface without GO, hydrophilic GO, hydrophobic rGO, and superhydrophobic rGO). As expected, *S. mutans* grows fast on the superhydrophobic surface of rGO-deposited Ti much the same as the control, which *S. mutans* was incubated in a culture dish because

Table 2 Average and STD of Water Contact Angle Taken for Three Samples on the Surface of Superhydrophobic, Hydrophobic and Hydrophilic Carbon Coating on Titanium Substrate

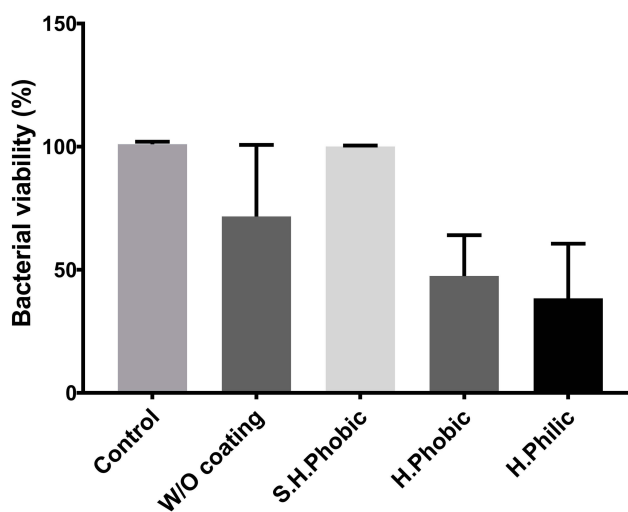| Surface	Average (°)	STD
Hydrophobic rGO	62	12.9
Super hydrophobic rGO	147.6	4.2
Hydrophilic GO	14	2.4
Ti substrate without coating	53	8.2

Figure 9 The effect of the various surface wettability on the viability of *Streptococcus mutans* which is a common anaerobic bacterium found in human oral cavity.
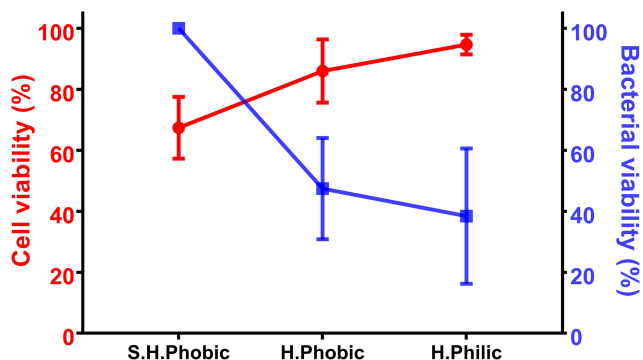
Figure 10 Biological application's comparison with different surface properties in terms of cells viability and antibacterial effect.

S. mutans is an anaerobic bacterium and proliferated well in anoxic environments. However, *S. mutans* on the hydrophilic surface grows slowly rather than on the bare-Ti surface. Therefore, the GO deposition with hydrophilicity enhanced the antibacterial effect and the biocompatibility on the Ti implant showing similarity with.[53]

Figure 10 is the diagrammatic representation of comparing surfaces with different wettability developing relationship with the cell viability and antibacterial effect. Cells viability and antibacterial effect for hydrophilic surface is 95% and 38%, respectively.

Conclusion

We report a very simple and novel method to effectively synthesize and convert hydrophobic surfaces into superhydrophobic and hydrophilic surfaces using high-density atmospheric plasma. Transition from hydrophobic (rGO) to hydrophilic (GO) surface is achieved by additional argon plasma treatment that results in highest biocompatibility as evaluated by MTT assay. Further, superhydrophobic surfaces are prepared using additional heat treatment; these surfaces show lowest cell viability. This simple, low cost, and highly productive synthesis method could enable cost-effective synthesis of rGO and GO for potential biological and photoelectrochemical applications. Our study showed that both rGO and GO did not show any cytotoxicity and in comparison GO showed higher cells viability and anti-bacterial effect.[53] Further rGO and GO will be used for different drug loading where rGO with hydrophobic character will be used for hydrophobic drugs while GO will be used for hydrophilic drugs. Additionally, osteoblast cells will be grown to check its differentiation into bone cells and will be followed for implant coating.

Disclosure
The authors report no conflicts of interest in this work.

References

1. Chung C, Kim Y-K, Shin D, Ryoo S-R, Hong BH, Min D-H. Biomedical applications of graphene and graphene oxide. *Acc Chem Res*. 2013;46(10):2211–2224. doi:10.1021/ar300159f
2. Chang H, Wu H. Graphene based nanomaterials: synthesis, properties, and optical and optoelectronic applications. *Adv Funct Mater*. 2013;23(16):1984–1997. doi:10.1002/adfm.201202460
3. Tiwari H, Karki N, Pal M, et al. Functionalized graphene oxide as a nanocarrier for dual drug delivery applications: the synergistic effect of quercetin and gefitinib against ovarian cancer cells. *Colloids Surf B Biointerfaces*. 2019;178:452–459. doi:10.1016/j.colsurfb.2019.03.037
4. Barra A, Ferreira NM, Martins MA, et al. Eco-friendly preparation of electrically conductive chitosan-reduced graphene oxide flexible bio-nanocomposites for food packaging and biological applications. *Compos Sci Technol*. 2019;173:53–60. doi:10.1016/j.compscitech.2019.01.027
5. Khan MM, Deen KM, Haider W. Combinatorial development and assessment of a Zr-based metallic glass for prospective biomedical applications. *J Non Cryst Solids*. 2019;523:119544. doi:10.1016/j.jnoncrysol.2019.119544
6. Khan MM, Nemati A, Rahman ZU, Shah UH, Asgar H, Haider W. Recent advancements in bulk metallic glasses and their applications: a review. *Crit Rev Solid State Mat Sci*. 2018;43(3):233–268. doi:10.1080/10408436.2017.1358149
7. Khan MM, Rahman ZU, Deen KM, Shabib I, Haider W. Sputtered Mg100-xZnx (0 ≤ x ≤ 100) systems as anode materials for a biodegradable battery aimed for transient bioelectronics. *Electrochim Acta*. 2020;329:135129. doi:10.1016/j.electacta.2019.135129
8. Khan MM, Shabib I, Haider W. A combinatorially developed Zr-Ti-Fe-Al metallic glass with outstanding corrosion resistance for implantable medical devices. *Scr Mater*. 2019;162:223–229. doi:10.1016/j.scriptamat.2018.11.011
9. Reina G, González-Domínguez JM, Criado A, Vázquez E, Bianco A, Prato M. Promises, facts and challenges for graphene in biomedical applications. *Chem Soc Rev*. 2017;46(15):4400–4416. doi:10.1039/C7CS00363C
10. Yi M, Shen Z. A review on mechanical exfoliation for the scalable production of graphene. *J Mater Chem A*. 2015;3(22):11700–11715. doi:10.1039/C5TA00252D
11. Brownson DA, Banks CE. The electrochemistry of CVD graphene: progress and prospects. *Phys Chem Chem Phys*. 2012;14(23):8264–8281. doi:10.1039/c2cp40225d
12. Mokhtar M, El Enein SA, Hassaan M, Morsy M, Khalil M. Thermally reduced graphene oxide: synthesis, structural and electrical properties. *Int J Nanoparticles Nanotechnol*. 2017;3(1):1–9. doi:10.35840/2631-5084/5508
13. Aziz M, Halim FSA, Jaafar J. Preparation and characterization of graphene membrane electrode assembly. *J Teknol*. 2014;69(9). doi:10.11113/jt.v69.3388

14. Novoselov KS, Fal'ko VI, Colombo L, Gellert PR, Schwab MG, Kim K. A roadmap for graphene. *Nature*. 2012;490:192. doi:10.1038/nature11458

15. Naghdi S, Rhee KY, Kim MT, Jaleh B, Park SJ. Atmospheric chemical vapor deposition of graphene on molybdenum foil at different growth temperatures. *Carbon Lett*. 2016;18:37–42. doi:10.5714/CL.2016.18.037

16. Fakhri P, Nasrollahzadeh M, Jaleh B. Graphene oxide supported Au nanoparticles as an efficient catalyst for reduction of nitro compounds and Suzuki–Miyaura coupling in water. *RSC Adv*. 2014;4 (89):48691–48697. doi:10.1039/C4RA06562J

17. Nasrollahzadeh M, Babaei F, Fakhri P, Jaleh B. Synthesis, characterization, structural, optical properties and catalytic activity of reduced graphene oxide/copper nanocomposites. *RSC Adv*. 2015;5 (14):10782–10789. doi:10.1039/C4RA12552E

18. Mohazzab BF, Jaleh B, Issaabadi Z, Nasrollahzadeh M, Varma RS. Stainless steel mesh-GO/Pd NPs: catalytic applications of Suzuki–Miyaura and Stille coupling reactions in eco-friendly media. *Green Chem*. 2019;21(12):3319–3327. doi:10.1039/C9GC00889F

19. Nasrollahzadeh M, Jaleh B, Jabbari A. Synthesis, characterization and catalytic activity of graphene oxide/ZnO nanocomposites. *RSC Adv*. 2014;4(69):36713–36720. doi:10.1039/C4RA05833J

20. Sali S, Mackey HR, Abdala AA. Effect of graphene oxide synthesis method on properties and performance of polysulfone-graphene oxide mixed matrix membranes. *Nanomaterials*. 2019;9(5):769. doi:10.3390/nano9050769

21. Somanathan T, Prasad K, Ostrikov K, Saravanan A, Krishna V. Graphene oxide synthesis from agro waste. *Nanomaterials*. 2015;5 (2):826–834. doi:10.3390/nano5020826

22. Nasrollahzadeh M, Atarod M, Jaleh B, Gandomirouzbahani M. In situ green synthesis of Ag nanoparticles on graphene oxide/TiO2 nanocomposite and their catalytic activity for the reduction of 4-nitrophenol, congo red and methylene blue. *Ceram Int*. 2016;42 (7):8587–8596. doi:10.1016/j.ceramint.2016.02.088

23. Jaleh B, Jabbari A. Evaluation of reduced graphene oxide/ZnO effect on properties of PVDF nanocomposite films. *Appl Surf Sci*. 2014;320:339–347. doi:10.1016/j.apsusc.2014.09.030

24. De S, Mohanty S, Nayak SK, Verma SK, Suar M. Nanotoxicity of rare earth metal oxide anchored graphene nanohybrid: a facile synthesis and in vitro cellular response studies. *Nano*. 2015;10 (6):1550091. doi:10.1142/S1793292015500915

25. Arun T, Verma SK, Panda PK, et al. Facile synthesized novel hybrid graphene oxide/cobalt ferrite magnetic nanoparticles based surface coating material inhibit bacterial secretion pathway for antibacterial effect. *Mater Sci Eng C*. 2019;104:109932. doi:10.1016/j.msec.2019.109932

26. Jaleh B, Shariati K, Khosravi M, Moradi A, Ghasemi S, Azizian S. Uniform and stable electrophoretic deposition of graphene oxide on steel mesh: low temperature thermal treatment for switching from superhydrophobicity to superhydrophobicity. *Colloids Surf a Physicochem Eng Asp*. 2019;577:323–332. doi:10.1016/j.colsurfa.2019.05.085

27. Chang T-K, Lu Y-C, Yeh S-T, Lin T-C, Huang C-H, Huang C-H. In vitro and in vivo biological responses to graphene and graphene oxide: a murine calvarial animal study. *Int J Nanomedicine*. 2020;15:647. doi:10.2147/IJN.S231885

28. Jaworski S, Sawosz E, Kutwin M, et al. In vitro and in vivo effects of graphene oxide and reduced graphene oxide on glioblastoma. *Int J Nanomedicine*. 2015;10:1585.

29. Guo X, Mei N. Assessment of the toxic potential of graphene family nanomaterials. *J Food Drug Anal*. 2014;22(1):105–115. doi:10.1016/j.jfda.2014.01.009

30. Nanda SS, Kim MJ, Yeom KS, An SSA, Ju H, Yi DK. Raman spectrum of graphene with its versatile future perspectives. *Trends Analyt Chem*. 2016;80:125–131. doi:10.1016/j.trac.2016.02.024

31. Johra FT, Lee JW, Jung WG. Facile and safe graphene preparation on solution based platform. *J Ind Eng Chem*. 2014;20(5):2883. doi:10.1016/j.jiec.2013.11.022

32. Sobon G, Sotor J, Jagiello J, et al. Graphene oxide vs. reduced graphene oxide as saturable absorbers for Er-doped passively mode-locked fiber laser. *Opt Express*. 2012;20(17):19463–19473. doi:10.1364/OE.20.019463

33. Thakur S, Karak N. Green reduction of graphene oxide by aqueous phytoextracts. *Carbon*. 2012;50(14):5331–5339. doi:10.1016/j.carbon.2012.07.023

34. Gurunathan S, Han JW, Park JH, et al. Reduced graphene oxide–silver nanoparticle nanocomposite: a potential anticancer nanotherapy. *Int J Nanomedicine*. 2015;10:6257. doi:10.2147/IJN.S92449

35. Shen Y, Lua AC. A facile method for the large-scale continuous synthesis of graphene sheets using a novel catalyst. *Sci Rep*. 2013;3:1–6. doi:10.1038/srep03037

36. Sahoo G, Polaki SR, Krishna NG, Kamruddin M. Electrochemical capacitor performance of TiO2 decorated vertical graphene nanosheets electrode. *J Phys D: Appl Phys*. 2019;52(37):375501. doi:10.1088/1361-6463/ab2ac5

37. Meng F, Song M, Wei Y, Wang Y. The contribution of oxygen-containing functional groups to the gas-phase adsorption of volatile organic compounds with different polarities onto lignin-derived activated carbon fibers. *Environ Sci Pollut Res*. 2019;26(7):7195–7204. doi:10.1007/s11356-019-04190-6

38. Ederer J, Janoš P, Ecorchard P, et al. Determination of amino groups on functionalized graphene oxide for polyurethane nanomaterials: XPS quantitation vs. functional speciation. *RSC Adv*. 2017;7 (21):12464–12473. doi:10.1039/C6RA28745J

39. Nanda SS, An SSA, Yi DK. Oxidative stress and antibacterial properties of a graphene oxide-cystamine nanohybrid. *Int J Nanomedicine*. 2015;10:549–556. doi:10.2147/IJN.S75768

40. Liu C, Liu H, Zhang K, et al. Partly reduced graphene oxide aerogels induced by proanthocyanidins for efficient dye removal. *Bioresour Technol*. 2019;282:148–155. doi:10.1016/j.biortech.2019.03.012

41. Sebastian N, Yu W-C, Hu Y-C, Balram D, Yu Y-H. Sonochemical synthesis of iron-graphene oxide/honeycomb-like ZnO ternary nanohybrids for sensitive electrochemical detection of antipsychotic drug chlorpromazine. *Ultrason Sonochem*. 2019;59:104696. doi:10.1016/j.ultsonch.2019.104696

42. Parvizi R, Azad S, Dashtian K, Ghaedi M, Heidari H. Natural source-based graphene as sensitising agents for air quality monitoring. *Sci Rep*. 2019;9(1):3798. doi:10.1038/s41598-019-40433-9

43. Gong X, Liu Y, Wang Y, et al. Amino graphene oxide/dopamine modified aramid fibers: preparation, epoxy nanocomposites and property analysis. *Polymer*. 2019;168:131–137. doi:10.1016/j.polymer.2019.02.021

44. Alam K, Sim Y, Yu J-H, et al. In-situ deposition of graphene oxide catalyst for efficient photoelectrochemical hydrogen evolution reaction using atmospheric plasma. *Materials*. 2020;13(1):12. doi:10.3390/ma13010012

45. Mageed AK, AB DR, Salmiaton A, et al. Preparation and characterization of nitrogen doped reduced graphene oxide sheet. *Int J Appl Chem*. 2016;12(1):104–108.

46. Bo Z, Shuai X, Mao S, et al. Green preparation of reduced graphene oxide for sensing and energy storage applications. *Sci Rep*. 2014;4:4684. doi:10.1038/srep04684

47. Choi MS, Lee SH, Yoo WJ. Plasma treatments to improve metal contacts in graphene field effect transistor. *J Appl Phys*. 2011;110 (7):073305. doi:10.1063/1.3646506

48. Depan D, Girase B, Shah JS. Structure–process–property relationship of the polar graphene oxide-mediated cellular response and stimulated growth of osteoblasts on hybrid chitosan network structure nanocomposite scaffolds. *Acta Biomater*. 2011;7(9):3432. doi:10.1016/j.actbio.2011.05.019

49. Kroning A, Furchner A, Adam S, et al. Probing carbonyl–water hydrogen-bond interactions in thin polyoxazoline brushes. *Biointerphases*. 2016;11(1):019001–019005. doi:10.1116/1.4939249

50. Gorbitz CH, Etter MC. Hydrogen bonds to carboxylate groups. The question of three-centre interactions. *J Chem Soc Perkin Trans 2*. 1992;2(1):131–135. doi:10.1039/P29920000131

51. Ganguly A, Sharma S, Papakonstantinou P, Hamilton J. Probing the thermal deoxygenation of graphene oxide using high-resolution in situ X-ray-based spectroscopies. *J Phys Chem C*. 2011;115 (34):17009–17019. doi:10.1021/jp203741y

52. Chenab KK, Sohrabi B, Rahmanzadeh A. Superhydrophobicity: advanced biological and biomedical applications. *Biomater Sci*. 2019;7(8):3110–3137. doi:10.1039/C9BM00558G

53. Gurunathan S, Han J, Morsy A, Eppakayala V, Kim J-H. Oxidative stress-mediated antibacterial activity of graphene oxide and reduced graphene oxide in Pseudomonas aeruginosa. *Int J Nanomedicine*. 2012;7:5901–5914. doi:10.2147/IJN.S37397